Available online at www.sciencedirect.com
ScienceDirect
Trans. Nonferrous Met. Soc. China 32(2022) 436−447
Transactions of Nonferrous Metals Society of China
www.tnmsc.cn

# Effect of pre-straining on structure and formation mechanism of precipitates in Al−Mg−Si−Cu alloy

Yao-yao WENG[1,2], Zhi-hong JIA[3,4], Li-peng DING[3], Jin LIAO[1], Ping-ping ZHANG[1], Ya-qi XU[1], Qing LIU[3,4]

1. School of Materials Science and Engineering, Nanjing Institute of Technology, Nanjing 211167, China;
2. Jiangsu Key Laboratory of Advanced Structural Materials and Application Technology, Nanjing Institute of Technology, Nanjing 211167, China;
3. Key Laboratory for Light-weight Materials, Nanjing Tech University, Nanjing 211816, China;
4. International Joint Laboratory for Light Alloys (Ministry of Education), College of Materials Science and Engineering, Chongqing University, Chongqing 400044, China

Received 22 February 2021; accepted 30 August 2021

**Abstract:** The effect of pre-straining on the structure and formation mechanism of precipitates in an Al−Mg−Si−Cu alloy was systematically investigated by atomic resolution high-angle annular dark-field scanning transmission electron microscopy (HAADF-STEM). Elongated and string-like precipitates are formed along the dislocations in the pre-strained Al−Mg−Si−Cu alloy. The precipitates formed along the dislocations exhibit three features: non-periodic atomic arrangement within the precipitate; Cu segregation occurring at the precipitate/$\alpha$(Al) interface; different orientations presented in one individual precipitate. Four different formation mechanisms of these heterogeneous precipitates were proposed as follows: elongated precipitates are formed independently in the dislocation; string-like precipitates are formed directly along the dislocations; different precipitates encounter to form string-like precipitates; precipitates are connected by other phases or solute enrichment regions. These different formation mechanisms are responsible for forming different atomic structures and morphologies of precipitates.

**Key words:** Al−Mg−Si−Cu alloy; pre-straining; Cu segregation; precipitate; HAADF-STEM

## 1 Introduction

Al−Mg−Si alloys are increasingly attractive as a candidate in automotive, aircraft and architecture applications. The increased popularity of Al−Mg−Si alloys is due to their high specific strength, good ductility, formability and corrosion resistance. These alloys display an obvious improvement in strength after artificial aging (AA) treatment because of the formation of nano-sized metastable precipitates [1−4]. The precipitation sequence of Al−Mg−Si alloy is usually considered as: SSSS → atomic clusters → GP zones → $\beta''$ → $\beta'$, $U1$, $U2$, $B'$ → $\beta$, Si [2,5,6]. Cu is often added to Al−Mg−Si alloys to increase the precipitation strengthening and the age hardening kinetics [7−9]. The precipitation sequence of Al−Mg−Si−Cu alloys is regarded as [10]: SSSS → atomic clusters → GP zones → $\beta''$, QP1, QP2, $C$ → $Q'$, QP2, $C$ → $Q$, Si.

SSSS represents the supersaturated solid solution. The needle-like $\beta''$ phase ($Mg_5Al_2Si_4$) is considered as the most important hardening precipitate for peak-aged Al−Mg−Si alloys [11,12]. While for the Al−Mg−Si−Cu alloys, $\beta''$, QP1, QP2 and $C$ phases coexist in the $\alpha$(Al) matrix during peak aging. The $Q'$ phase and the $\beta'$ phase ($Mg_9Si_5$) have hexagonal space group and multiple orientation relationships (ORs) with the $\alpha$(Al) matrix [13−15]. The $C$ phase has a monoclinic

**Corresponding author:** Yao-yao WENG, E-mail: yaoyaoweng@njit.edu.cn; Li-peng DING, E-mail: lipeng.ding@njtech.edu.cn
DOI: 10.1016/S1003-6326(22)65805-9

lattice and a constant OR of $[001]_C//[001]_\alpha$, $(010)_C//(\bar{1}50)_\alpha$ [16]. All metastable precipitates in the Al−Mg−Si(−Cu) alloys are structurally related through a common QP lattice (which is also named as Si-network by MARIOARA et al [17]) with a projected near hexagonal symmetry of $a=b\approx0.4$ nm, and $c=0.405$ nm [17,18].

Pre-straining is widely used in industry to increase the mechanical properties of aluminum alloys [19−21]. Firstly, pre-straining can relieve the residual stress induced by quenching and improve the plasticity of alloys. The compressive stress induced by quenching can be neutralized by the tensile stress of the pre-straining. Secondly, the introduced dislocations can provide a heterogeneous nucleation site for the precipitation resulting in an acceleration of the precipitation kinetics [22]. The influence of pre-straining on the microstructure and properties of Al−Mg−Si(−Cu) alloys has been investigated in detail. QUAINOO and YANNACOPOULOS [23] found that AA6111 develops increased strength with increasing levels of pre-straining during natural aging. BIROL and KARLIK [24] reported that the pre-straining after solutionizing suppresses the adverse effect of natural aging and promotes the precipitation of $\beta''$ phase in a twin-roll cast 6062 sheet. YASSAR et al [25] found that the introduction of dislocation changes the precipitate type for the AA6022 alloy from $\beta''$ to $\beta'$ and $Q'$. TEICHMANN et al [26,27] suggested that the pre-aging deformation suppresses the growth of GP zones and $\beta''$ phases, and promotes the formation of elongated and conjoined precipitates along dislocation lines. SAITO et al [28] found that parts of unit cells of the $Q'$ phase are formed at the end of a string-type precipitate that extends along the dislocation line. Recently, LAI et al [29] have revealed that the majority of precipitates in the deformed Al−Mg−Si alloys are short-range ordered while long-range disordered precipitates and composite precipitates.

Most of the reports related to pre-straining focused on the effect of dislocation on the microstructure (such as size and morphology) and properties of Al−Mg−Si alloys, while the effect of dislocation on the structural evolution of precipitate received less attention. The following questions are still not clear: firstly, the atomic structures of precipitates formed along dislocations are elusive. Although the "string-like" phases formed at the dislocations have been reported, the atomic structures of these "string-like" phases are not clear. Secondly, most of the investigations about pre-straining are performed on the Al−Mg−Si alloys, while the effect of pre-straining on the precipitation behavior of Al−Mg−Si−Cu alloys is less studied. Thirdly, the formation mechanism of elongated precipitate in the pre-deformed alloy is not fully understood. Understanding the influence mechanism of pre-straining on the atomic structure of precipitate is essential for expanding the application of pre-straining in Al−Mg−Si−Cu alloys. Therefore, in the present work, transmission electron microscopy (TEM) and atomic-resolution high-angle annular dark-field scanning transmission electron microscopy (HAADF-STEM) were used to investigate the effect of pre-straining on the atomic structures of precipitates in an Al−Mg−Si−Cu alloy. The precipitation behavior for the pre-strained Al−Mg−Si−Cu alloy and the influence mechanism of pre-deformation in precipitation were explored.

## 2 Experimental

An alloy with a chemical composition of Al−1.11Mg−0.67Si−0.5Cu (wt.%) was used in this study. The alloy was cast into a slab ingot from high-purity Al (99.9%), high-purity Mg (99.9%), Al−10wt.%Si and Al−49.5wt.%Cu master alloys by using an induction furnace. The chemical composition of the alloy was measured by optical emission spectroscopy. The ingot was homogenized at 560 °C for 6 h in an air furnace which was heated with a heating rate of 50 °C/min from a room temperature, and subsequently naturally cooled. The ingot was then hot- and cold-rolled to a 1 mm-thick sheet. The sheet was solution heat-treated at 570 °C for 20 min in a muffle furnace and water-quenched to room temperature. Then, pre-straining (0 and 10%) was performed immediately after quenching. All samples were then artificially aged at 180 °C for 4 h. A schematic representation of the heat treatment procedure is shown in Fig. 1.

The microstructures of the Al−Mg−Si−Cu alloys in different pre-straining conditions were investigated by an FEI Tecnai G2 F20 TEM. Atomic resolution HAADF-STEM characterization was performed using a spherical aberration probe corrected FEI Titan G2 60−300 ChemiSTEM with a

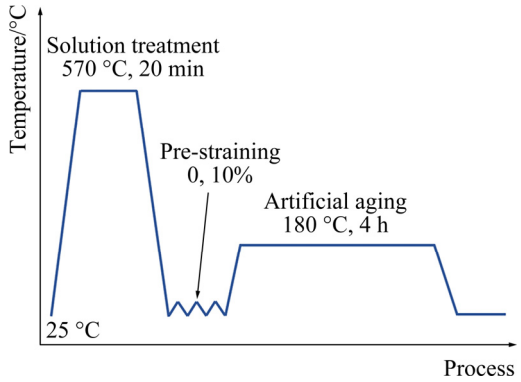


**Fig. 1** Schematic of heat treatment procedure

Schottky field emitter operated at 300 kV. The probe diameter was 0.08 nm, and a 21 mrad convergence semi-angle and a spot size 7 were used for HAADF imaging. All TEM images were taken along the $\langle 001 \rangle_{\alpha}$ zone axis. All HAADF-STEM images were Fourier filtered with an aperture encompassing all the visible spots in the Fourier transform. In order to ensure the accuracy of the data of precipitates, at least 10 TEM bright-field images and 100 HAADF-STEM images were taken to compare and make statistical comparisons. Disc-shaped TEM specimens were prepared by electro polishing using a Struers TenuPol−5 device with an electrolyte of 33 vol.% $HNO_3$ in methanol at a temperature about −30 °C.

## 3 Results

### 3.1 TEM characterization

Figure 2 shows TEM bright-field images of the pre-strained and non-pre-strained Al−Mg−Si−Cu samples after AA at 180 °C for 4 h. For the non-pre-strained alloy, large numbers of rod-like and lath-like precipitates are homogeneously distributed in the $\alpha$(Al) matrix, which could be called as a conventional phase. Compared with the non-pre-strained alloy, the pre-strained alloy presents heterogeneous string-like and elongated precipitates along the dislocations as shown in Figs. 2(b, c), which exhibit large size and could be called as an unconventional phase. Besides, the precipitates formed in the pre-strained alloy present a refined distribution compared with that of the non-pre-strained alloy. These results demonstrate that pre-straining can facilitate the formation of precipitates and change their morphologies for the Al−Mg−Si−Cu alloy.

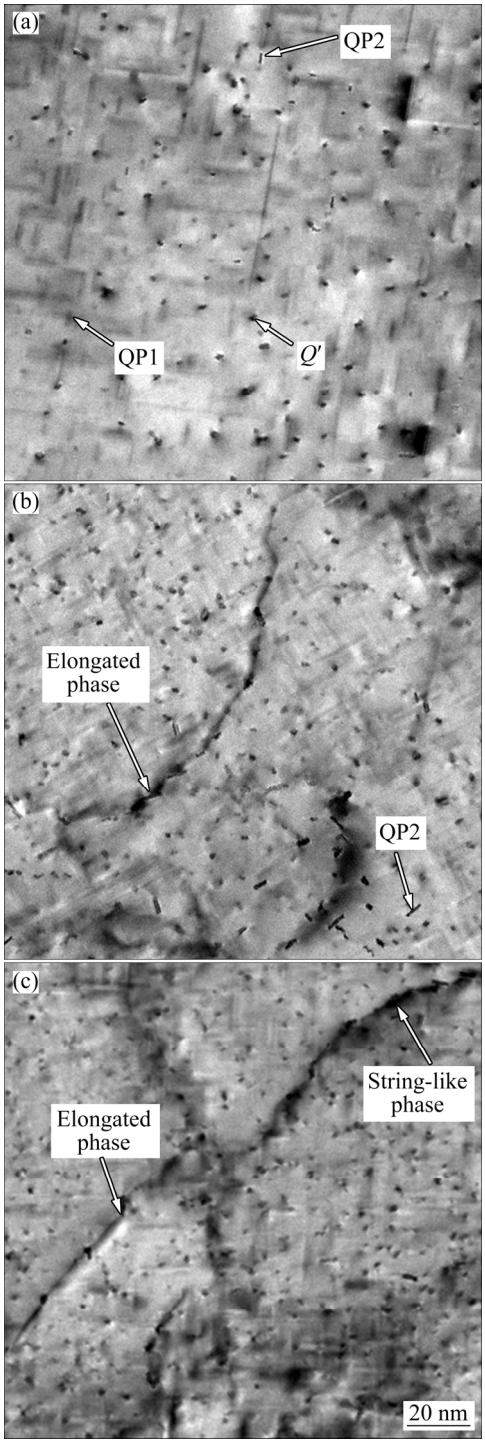


**Fig. 2** TEM bright-field images of various pre-strained Al−Mg−Si−Cu samples after artificial aging at 180 °C for 4 h: (a) Non-pre-strained; (b, c) 10% pre-strained

### 3.2 HAADF-STEM characterization

3.2.1 Precipitates formed in non-pre-strained alloy

Atomic resolution characterization was carried out for these precipitates formed in the pre-strained and non-pre-strained Al−Mg−Si−Cu alloys. Figure 3 shows HAADF-STEM images and the

corresponding fast Fourier transforms (FFT) patterns of the precipitates formed in the non-pre-strained alloy. Due to the intensity of HAADF-STEM images varying approximately as the square of atomic number, $Z^2$, Cu column could be easily identified for its strong atomic number relative to other elements ($Z$=29 for Cu, $Z$=13 for Al, $Z$=12 for Mg, and $Z$=14 for Si). It is clear that all the three precipitates have a non-periodic atomic arrangement, but some short-range orders are visible as evidenced by the FFT pattern presented in Figs. 3(b, d, f). In Fig. 3(a), a composite precipitate containing substructures of low density cylinder (LDC) and Cu sub-unit clusters is formed. The LDC, which consists of nine atomic columns with four-fold symmetry, is the main substructure of the $\beta''$ phase. The precipitates presented in Figs. 3(c, e) can be identified as QP1 and QP2 phases, respectively, as evidenced by the existence of the common QP lattice and the $Q'/C$ unit cells within the precipitates. The QP2 phase has the OR of $[001]_{QP2}//[001]_{\alpha}$, $(010)_{QP2}//(\bar{1}50)_{\alpha}$ and $(100)_{QP2}//(100)_{\alpha}$. According to the previous literature [16], the $(010)_{\alpha}$ habit plane of QP2 phase is coherent with the $\alpha$(Al) matrix, while the $(100)_{\alpha}$ plane (end region of precipitate) is partially coherent. In these disordered

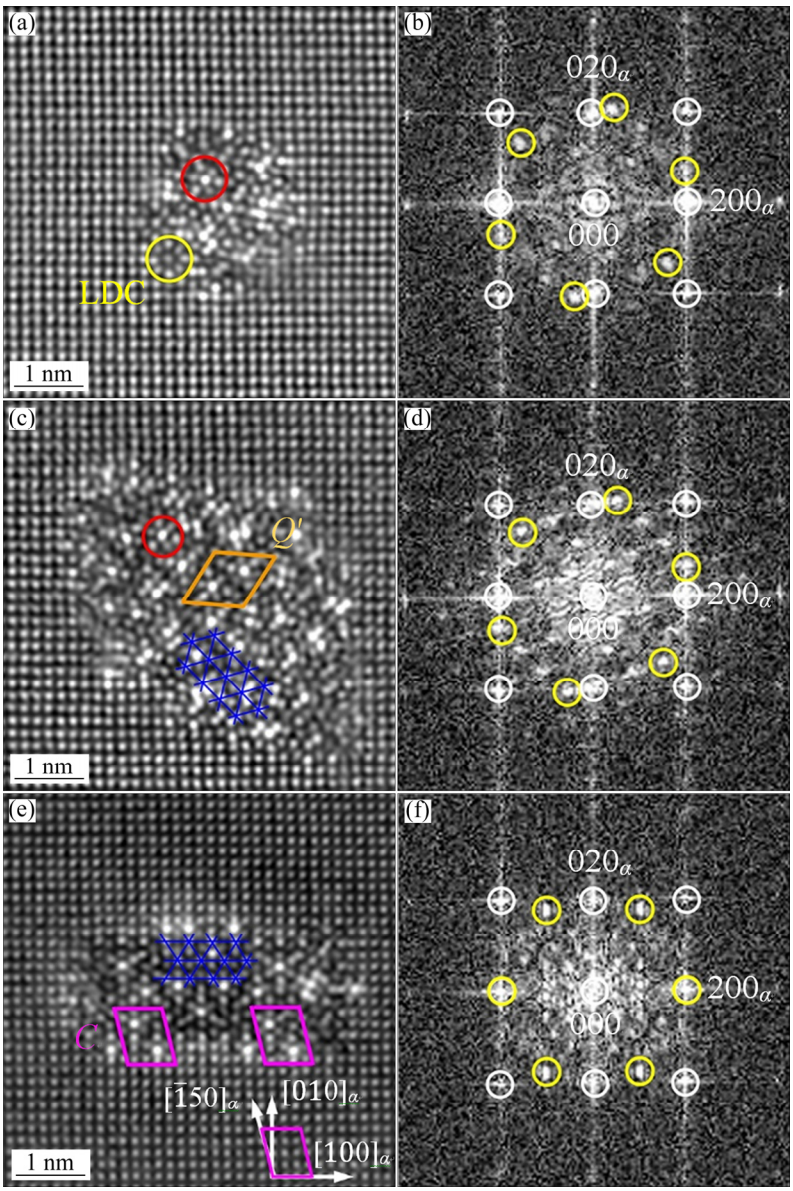


**Fig. 3** HAADF-STEM images and corresponding FFT patterns of precipitates formed after 4 h AA for non-pre-strained Al−Mg−Si−Cu alloy: (a, b) Composite phase; (c, d) QP1 phase; (e, f) QP2 phase (The QP lattice is marked by blue lines and the Cu sub-unit clusters are marked by red circles. The QP spots in the FFT pattern are marked by yellow circles, and the lattice of Al matrix is marked by white circles)

phases, most of Cu atoms enter into the interior of precipitates, while no Cu segregation is observed at the precipitate/$\alpha$(Al) interfaces.

3.2.2 Precipitates formed in pre-strained alloy

In order to investigate the influence of pre-straining on the atomic structure of precipitate, HAADF-STEM characterization was performed for the precipitates formed along dislocations. Figure 4 shows the low-resolution HAADF-STEM images of these heterogeneous precipitates. The discontinuous and continuous precipitates can be clearly observed along the dislocations, while the dislocation lines are not visible in the HAADF-STEM mode. Most of the precipitates have elongated and string-like morphologies. By analyzing the contrast of atomic columns, it can be seen that most of Cu atoms are segregated at the precipitate/$\alpha$(Al) interfaces, while the concentration of Cu atoms in the interior of precipitates is much lower. This is different from the precipitates formed in the non-pre-strained alloy, in which most of the Cu atoms are incorporated in the interior of precipitates.

Figure 5 shows the HAADF-STEM images of the elongated precipitates formed along the dislocations for the pre-strained Al−Mg−Si−Cu alloy. Similar to the precipitates formed in the non-pre-strained alloy, these elongated precipitates also exhibit disordered structures which contain different types of unit cells and substructures. In more details, for the precipitate shown in Fig. 5(a), the $U2$ unit cell, LDC and Cu sub-unit clusters can be seen. In Fig. 5(b), the $\beta'$ unit cell coexists with the Cu sub-unit clusters, while in Fig. 5(c), the $Q'$ and $\beta'$ unit cells are observed within one precipitate. The main difference between the elongated precipitates formed along the dislocations and the precipitates formed in the non-pre-strained alloy are as follows. (1) Except for the $Q'$ unit cell, the $\beta'$ and $U2$ unit cells are also formed in the elongated precipitates, while these unit cells are not observed for the precipitates in the non-pre-strained alloy. (2) For the elongated precipitates in the pre-strained alloy, most of Cu atoms segregate at the precipitate/$\alpha$(Al) interfaces by occupying the Si positions in the QP lattice or the Al positions in the $\alpha$(Al) matrix. While for the non-pre-strained alloy, most of Cu atoms are incorporated in the interior of precipitates. The formation of $\beta'$ and $U2$ unit cells is supposed to be induced by the low concentration of Cu atoms in the interior of precipitates, which mainly results from the Cu segregation at the precipitate/$\alpha$(Al) interfaces.

Figure 6 shows HAADF-STEM images and corresponding FFT patterns of the lath-like QP2 phases formed along the dislocations. The $\beta'$ unit cell, $C$ unit cell and Cu sub-unit cluster are coexistent within the QP2 phases. No clear difference is found between the QP2 precipitates

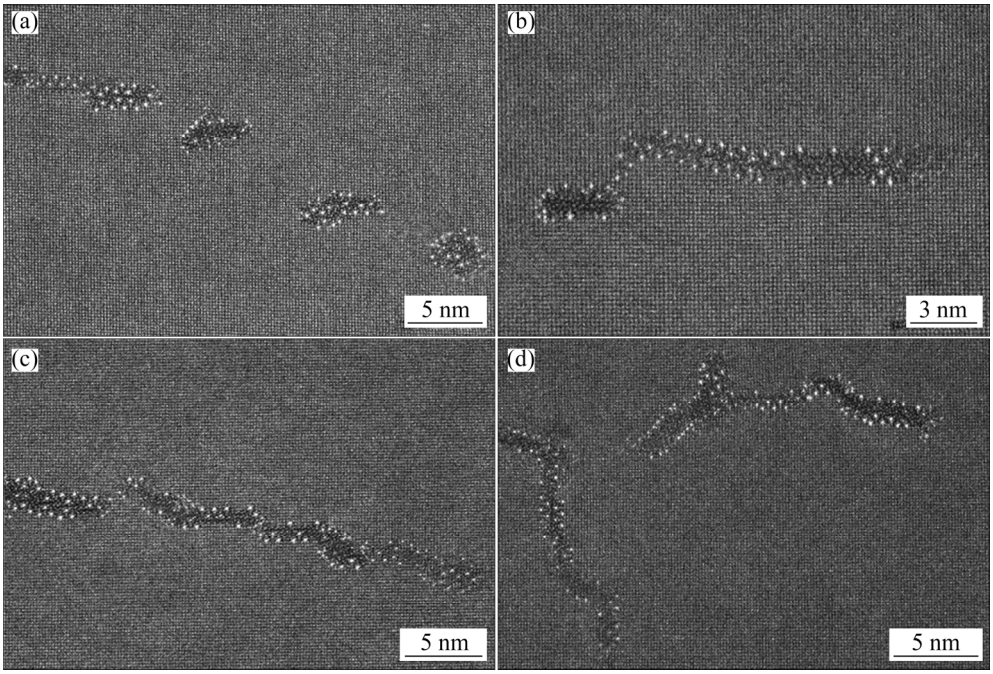


**Fig. 4** Low-resolution HAADF-STEM images of precipitates formed related to dislocations for pre-strained Al−Mg−Si−Cu alloy: (a) Discontinuous elongated precipitates; (b−d) Continuous string-like precipitates

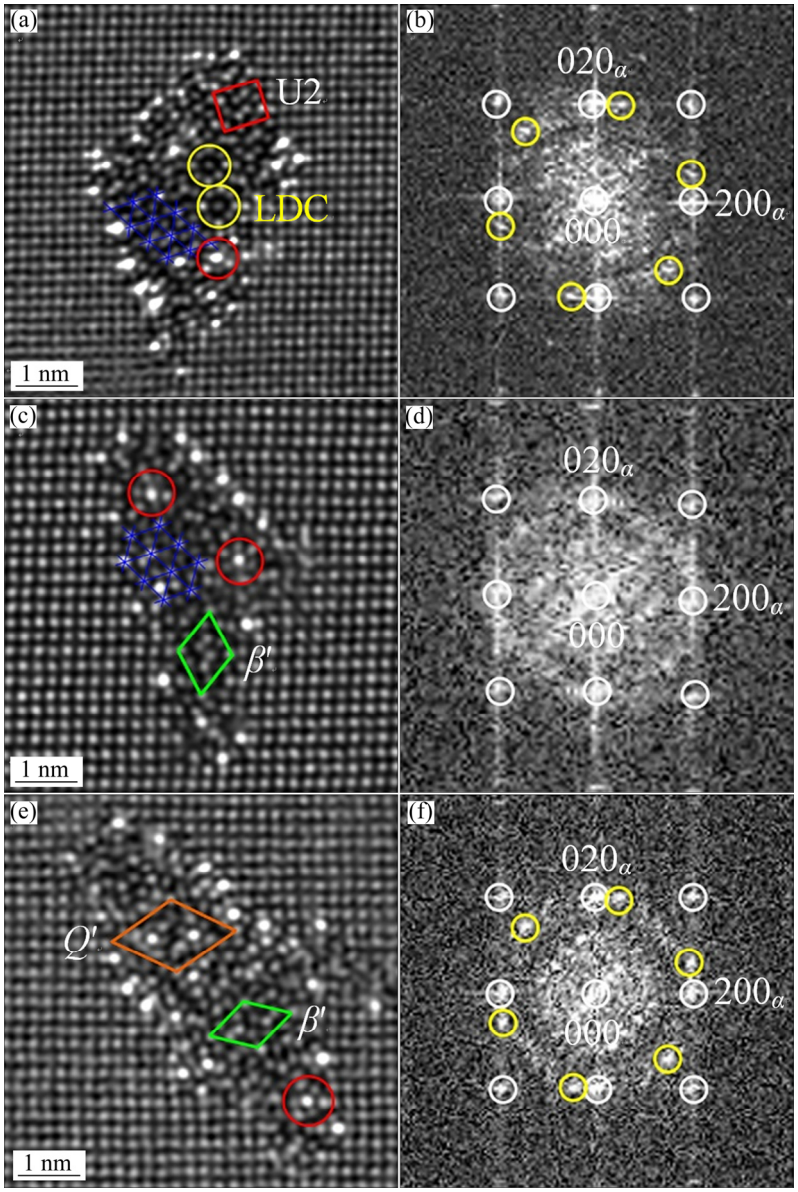


**Fig. 5** HAADF-STEM images (a, c, e) and corresponding FFT patterns (b, d, f) of elongated precipitates formed in dislocations for pre-strained Al−Mg−Si−Cu alloy (The LDC and Cu sub-unit clusters are marked by yellow and red circles, respectively. The QP lattice is marked by blue lines. The QP spots in the FFT pattern are marked by yellow circles, and the lattice of Al matrix is marked by white circles)

formed in the dislocations for the pre-strained alloy and the $\alpha$(Al) matrix for the non-pre-strained alloy [16].

Except for the rod-like and lath-like precipitates, the string-like precipitates are the most common precipitates formed in the dislocations. Figure 7(a) shows the atomic resolution HAADF-STEM image of a string-like precipitate. It can be seen that this string-like precipitate exhibits a zigzag morphology with different unit cells in different regions. On the left side of the precipitate (Fig. 7(b)), this region can be identified as QP2 phase as evidenced by the formation of *C* unit cells. The arrangement of *C* unit cells is nonperiodic: each *C* unit cell is separated and aligned in different atomic planes. The habit plane of the QP2 phase formed in this region is identified as $(160)_\alpha$, which is about 10°-tilted compared with that of the QP2 phase ($(010)_\alpha$ plane) formed in the $\alpha$(Al) matrix. While the OR of *C* unit cell in this region is not changed, as $[001]_C//[001]_\alpha$, $(010)_C//(\bar{1}50)_\alpha$. Thus, it can be deduced that the tilted habit plane of the QP2 phase is due to the *C* unit cells arranging along the dislocations. In the middle region (Fig. 7(c)),

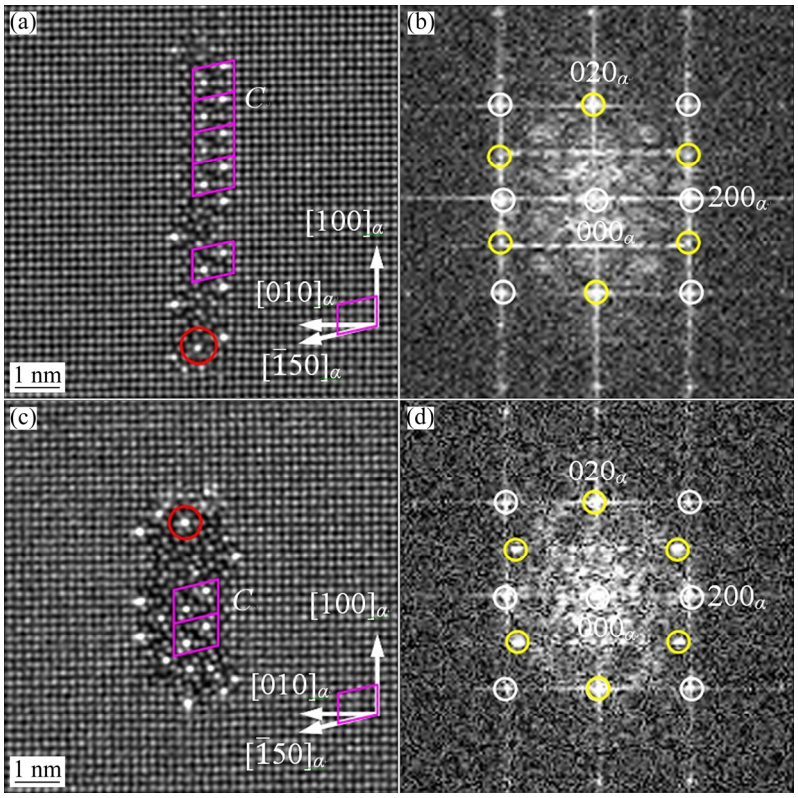


**Fig. 6** HAADF-STEM images (a, c) and corresponding FFT patterns (b, d) of lath-like QP2 precipitates formed in dislocations for pre-strained Al−Mg−Si−Cu alloy (The Cu sub-unit clusters are marked by red circles. The QP spots in the FFT pattern are marked by yellow circles, and the lattice of Al matrix is marked by white circles)

the LDC and Cu sub-unit clusters are formed at the precipitate/$\alpha$(Al) interfaces. Besides, the structure of Cu sub-unit clusters is changed in this region. Figures 7(h−j) show three distorted Cu-cluster zones at the interfaces. In the first case shown in Fig. 7(h), the Mg atomic column with higher contrast is supposed to contain Cu atoms for the Cu sub-unit cluster. In the second case as shown in Fig. 7(i), the Cu sub-unit cluster formed in the precipitate/$\alpha$(Al) interface presents a distorted Al-fcc structure on one side of this substructure. The last case in Fig. 7(j) is three Mg atoms and three Si atoms surrounding a Cu atom, which is the most common Cu sub-unit clusters formed in the precipitates. On the right side (Fig. 7(d)), it is obvious that the *U*2 unit cell is formed in the interior, while the Cu segregation and Cu sub-unit clusters can be observed at the precipitate/$\alpha$(Al) interfaces. The precipitate shown in Fig. 7(d) extends along the $[830]_\alpha$ direction, which is about 20°-rotation related to the $[100]_\alpha$ direction. The hexagonal QP lattice, acting as a skeleton structure of the string-like precipitate, exhibits different orientations in different regions of the precipitate. The angle of $[100]_{QP}$ lattice with its nearest $[100]_\alpha$ is termed as "QP-angle". The QP-angle of the QP lattice in Fig. 7(b) is about 0°, while it is about 12° in Fig. 7(d). These results indicate that the string-like precipitate has different ORs in different regions.

Figure 8 shows HAADF-STEM images of two string-like precipitates formed in the dislocations. It can be clearly seen in Fig. 8(a) that this string-like precipitate consists of lath-like QP2 precipitates formed in different atomic planes, and these QP2 precipitates are connected by disordered structure with low Cu concentration. The *C* unit cell is clearly observed in the QP2 phase as marked by purple lines. Enlarged HAADF-STEM image of the connected region is presented in Fig. 8(b), and two pairs of atomic columns with bright contrast between the Si and Cu columns are formed. These double columns are similar to the $Si_2$ columns formed in $\beta''$ (the $Si_2$ column is suggested as a stable skeleton of $\beta''$ phases). Some Cu atoms are expected to be incorporated in the $Si_2$ columns as higher contrast is involved. The double columns are supposed to be formed in the early stage of aging,

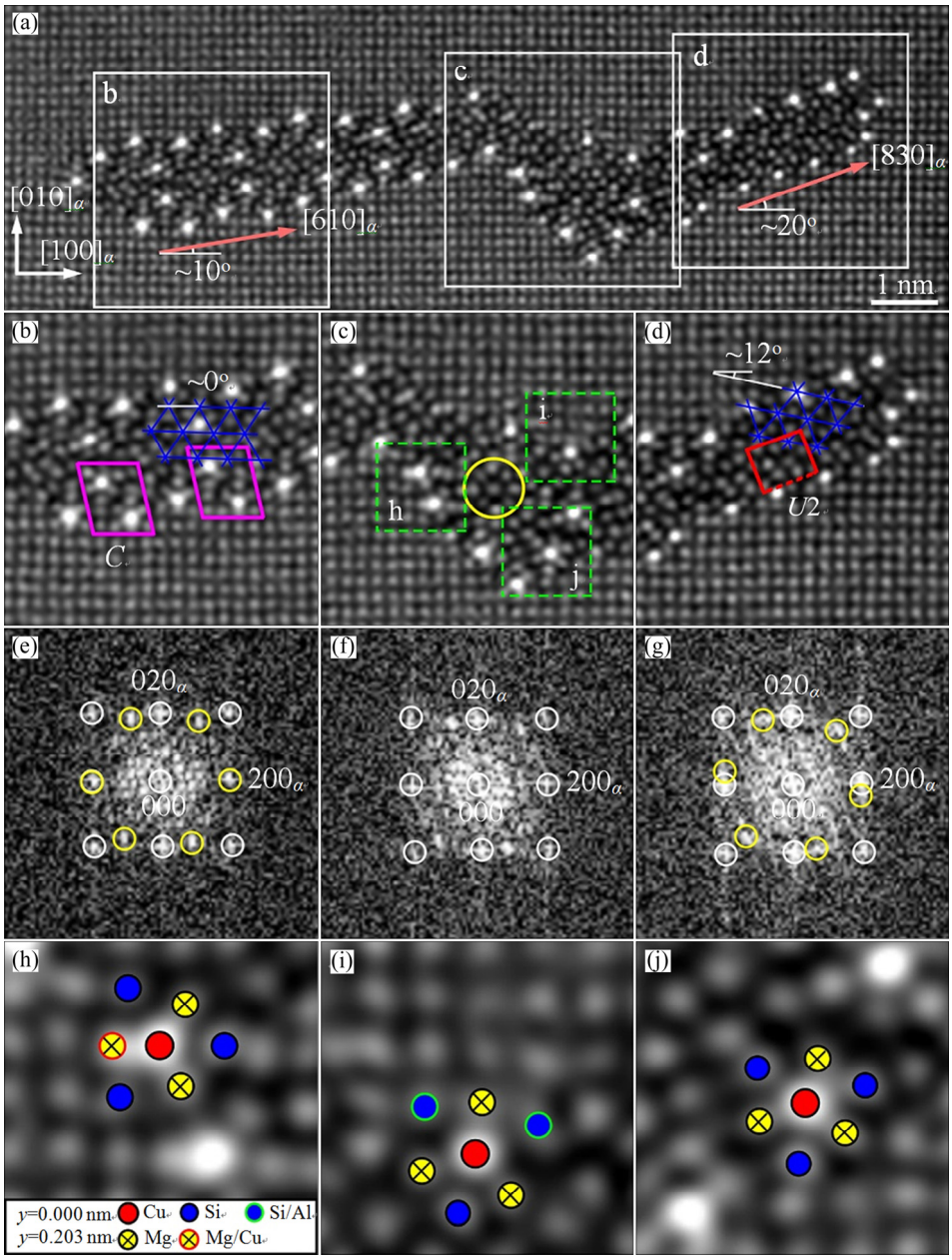


**Fig. 7** HAADF-STEM image of string-like precipitate formed in dislocation for pre-strained Al−Mg−Si−Cu alloy (a), enlarged HAADF-STEM images (b−d) of zones marked in (a), corresponding FFT patterns (e−g) of (b−d), respectively, and enlarged HAADF-STEM images (h−j) of zones marked in (c) (The QP lattice is marked by blue lines and the LDC and Cu sub-unit clusters are marked by yellow and red circles, respectively, the QP spots in the FFT pattern are marked by yellow circles, and the lattice of Al matrix is marked by white circles)

prior to the formation of QP2 phase. In Fig. 8(c), the QP2 precipitates formed in the $(100)_\alpha$ and $(010)_\alpha$ planes are connected. For the QP2 phase along the $[010]_\alpha$ direction, the *C* unit cells are formed in different parallel planes, leading to a non-periodic arrangement of *C* unit cells in the QP2 precipitate. Figure 8(d) shows enlarged HAADF-STEM image of the connected region marked in Fig. 8(c). It can be seen that two precipitates are connected by a string of atoms with distorted Al-fcc structure. These distorted atoms are supposed to result from Mg or Si atoms enriching in the dislocations. Therefore, it can be deduced that the isolated lath-like QP2 precipitates are formed in the dislocation firstly, and then enrichment of solute atoms or nucleation of precipitates occurs in the gap of two QP2 phases to connect these precipitates.

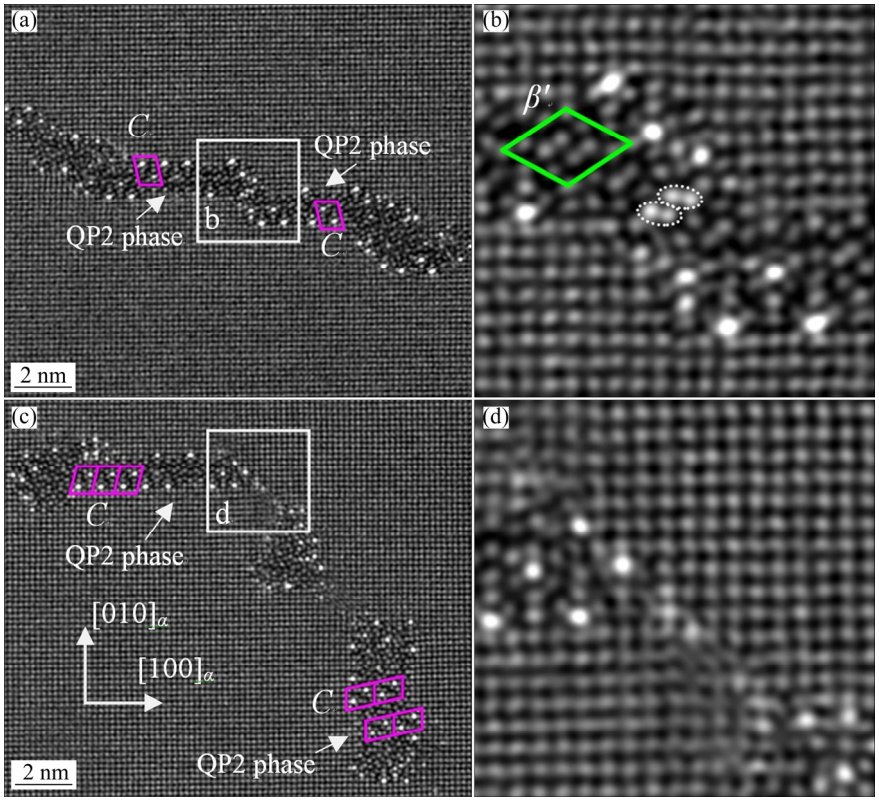


**Fig. 8** String-like phases distributed in dislocations (a, c) and enlarged HAADF-STEM images (b, d) of zones marked in (a, c), respectively

## 4 Discussion

### 4.1 Influence mechanism of pre-straining on precipitate structure

Based on the microstructural characterizations, the influence of pre-straining on precipitate structures of an Al−Mg−Si−Cu alloy can be listed as follows. Firstly, the precipitates formed in the pre-strained alloy are finer and denser than those of the non-pre-strained alloy. This is because the introduced dislocations can provide heterogeneous nucleation sites for the precipitates [29,30], resulting in an acceleration of precipitation kinetics. Secondly, all the precipitates formed in the dislocations exhibit elongated or string-like morphologies, while the precipitates formed in the $\alpha$(Al) matrix have rod-like or lath-like morphologies. Besides, the precipitates formed in the dislocations have a larger size than those in the $\alpha$(Al) matrix. This is because the high free energy and diffusion rate of dislocations facilitate the growth of precipitates along the dislocation to form the elongated and string-like morphologies [31]. Thirdly, the atomic structures of precipitates formed in the dislocations are changed, the following characteristics can be listed. (1) All precipitates have a non-periodic atomic arrangement, and disordered structures prevail within these precipitates. Different unit cells and substructures, such as the $Q'$ and $C$ unit cells, LDC and Cu sub-unit clusters, and even the $U2$ and $\beta'$ unit cells which are not supposed to be formed in precipitates of Al−Mg−Si−Cu alloy [32], could coexist in the elongated precipitates for the pre-strained alloy. (2) For the precipitates formed in the dislocations, most of Cu atoms are segregated at the precipitate/$\alpha$(Al) interfaces by occupying the Si positions in the QP lattice or the Al positions in the $\alpha$(Al) matrix. While in the non-pre-strained alloy, most of Cu atoms are incorporated in the interior of precipitates. The main reason for this segregation is probably that the introduced dislocations change the stress field around the precipitates, and then Cu segregation at the precipitate/$\alpha$(Al) interface occurs to decrease the strain energy of the precipitates. The Cu segregation at the interface can also decrease the Cu concentration in the interior of precipitate, which leads to the formation of $\beta'$ and $U2$ unit cells [32]. (3) Different ORs are identified within

one individual precipitate. The habit plane of precipitate is changed to adapt the direction of dislocation. It is supposed that the precipitates (or fragments) with different ORs initially nucleate along the dislocation lines, and later on these fragments are connected to form one string-like precipitate with multiple ORs.

### 4.2 Nucleation mechanism of precipitates in dislocations

For the nucleation mechanism of heterogeneous precipitates formed in the dislocations, four different mechanisms can be proposed based on the above experimental investigations. The schematic illustrations of the transformation paths of the elongated and string-like precipitates in the pre-strained Al−Mg−Si−Cu alloy are shown in Fig. 9. In Case 1 (Fig. 9(a)), rod-like or lath-like precipitates are formed independently in different regions of the dislocation, and then these precipitates grow along the dislocation to form elongated precipitates, as seen from the precipitates presented in Fig. 5. In Case 2 (Fig. 9(b)), a string-like precipitate is formed directly along the dislocation, and different unit cells or substructures can be found in different regions of the precipitate, as seen from the precipitate presented in Fig. 7(a). In Case 3 (Fig. 9(c)), lath-like or elongated-like precipitates are firstly nucleated in different regions of the dislocation, and then these precipitates are encountered to form a string-like precipitate during the growth of these isolated precipitates, as seen from the precipitate presented in Fig. 8(a). In Case 4 (Fig. 9(d)), lath-like or elongated-like precipitates are firstly nucleated in different regions of the dislocation, and then these precipitates are connected by another precipitate or solute enrichment regions in the gap of two isolated precipitates, as seen from the precipitate presented in Fig. 8(c). The four different mechanisms are responsible for the formation of precipitates with different structures and morphologies. These results provide new insights in controlling the precipitation hardening of the Al−Mg−Si−Cu alloy by pre-straining.

## 5 Conclusions

(1) Compared with the no-pre-strained alloy, the pre-strained Al−Mg−Si−Cu alloy has finer and denser precipitates in the $\alpha$(Al) matrix. Elongated and string-like precipitates are formed along the

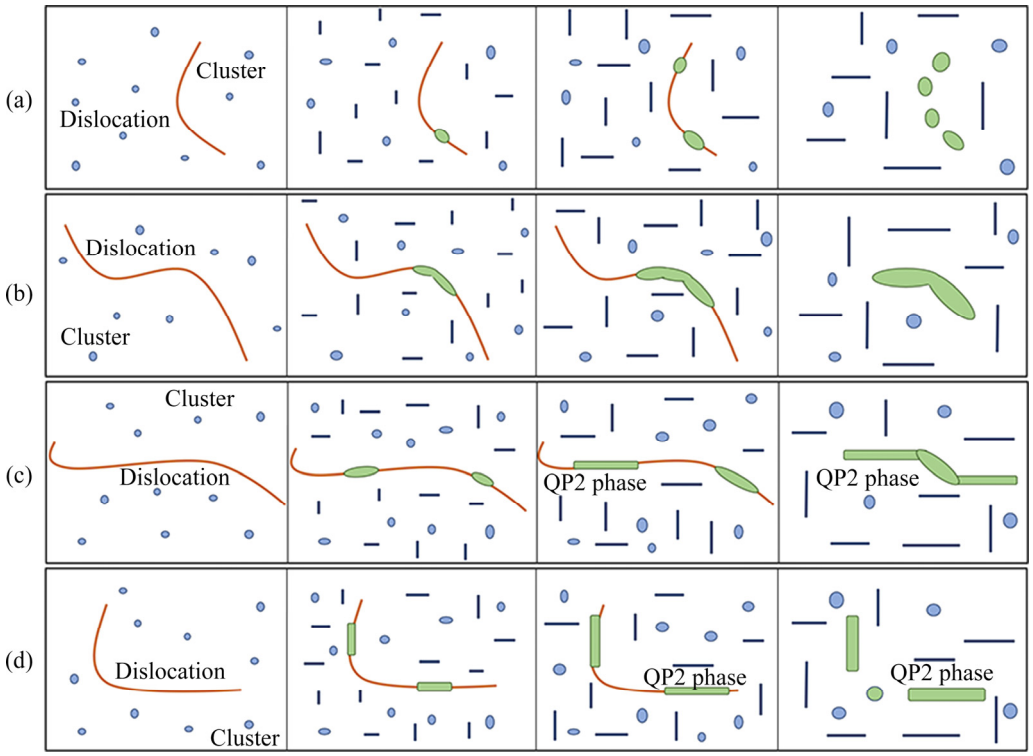


**Fig. 9** Schematic illustration of transformation paths of precipitates for pre-strained Al−Mg−Si−Cu alloy (Dislocations are marked by orange lines, precipitates formed in dislocations and $\alpha$(Al) matrix are marked by green and blue particles, respectively)

dislocations in the pre-strained alloy.

(2) The atomic structures of precipitates formed in the dislocations have three features: non-periodic atomic arrangement in the interior of precipitate; most of Cu atoms segregating at the precipitate/$\alpha$(Al) interfaces; different orientations present in one individual precipitate.

(3) Four formation mechanisms of the precipitates in the dislocations are proposed as follows: elongated precipitates are formed independently in the dislocations; string-like precipitates are formed directly along the dislocations; different precipitates encounter to form string-like precipitates; precipitates are connected by another phase or solute enrichment regions.

## Acknowledgments

This work was financially supported by the Natural Science Foundation of Jiangsu Province, China (No. BK20201035), the Talent Research Fund in Nanjing Institute of Technology, China (No. YKJ201957), the National Natural Science Foundation of China (Nos. 51871035, 52001159), and the Natural Science Foundation of the Jiangsu Higher Education Institutions of China (Nos. 20KJB430016, 20KJB430012).

## References

[1] EDWARDS G A, STILLER K, DUNLOP G L, COUPER M J. The precipitation sequence in Al−Mg−Si alloys [J]. Acta Materialia, 1998, 46: 3893−3904.

[2] SAITO T, EHLERS F J H, LEFEBVRE W, HERNANDEZ-MALDONADO D H, BJØRGE R, MARIOARA C D, ANDERSEN S J, HOLMESTAD R. HAADF-STEM and DFT investigations of the Zn-containing $\beta''$ phase in Al−Mg−Si alloys [J]. Acta Materialia, 2014, 78: 245−253.

[3] WANG Xiang-dong, LIU Xiong, DING Hao, YAN Su-rong, XIE Zi-hua, PAN Bai-qing, LI Yong-hong, PAN Qing-lin, DENG Yun-lai, WANG Wei-yi. Microstructure and mechanical properties of Al−Mg−Si alloy U-shaped profile [J]. Transactions of Nonferrous Metals Society of China, 2020, 30: 2915−2926.

[4] WANG Xiao-feng, GUO Ming-xing, PENG Wen-fei, WANG Yong-gang, ZHUANG Lin-zhong. Relationship among solution heating rate, mechanical properties, microstructure and texture of Al−Mg−Si−Cu alloy [J]. Transactions of Nonferrous Metals Society of China, 2021, 31: 36−52.

[5] CHEN Hao-nan, LU Jiang-bo, KONG Yi, LI Kai, YANG Tong, MEINGAST A, YANG Ming-jun, LU Qiang, DU Yong. Atomic scale investigation of the crystal structure and interfaces of the $\beta'$ precipitate in Al−Mg−Si alloys [J]. Acta Materialia, 2020, 185: 193−203.

[6] VISSERS R, van HUIS M A, JANSEN J, ZANDBERGEN H W, MARIOARA C D, ANDERSEN S J. The crystal structure of the $\beta'$ phase in Al−Mg−Si alloys [J]. Acta Materialia, 2007, 55: 3815−3823.

[7] MØRTSELL E A, MARIOARA C D, ANDERSEN S J, RØYSET J, REISO O, HOLMESTAD R. Effects of germanium, copper, and silver substitutions on hardness and microstructure in lean Al−Mg−Si alloys [J]. Metallurgical and Materials Transactions A, 2015, 46: 4369−4379.

[8] JIA Zhi-hong, DING Li-peng, CAO Ling-fei, SANDERS R, LI Shi-chen, LIU Qing. The influence of composition on the clustering and precipitation behavior of Al−Mg−Si−Cu alloys [J]. Metallurgical and Materials Transactions A, 2017, 48: 459−473.

[9] WANG Xiao-feng, SHI Tong-ya, WANG He-bin, ZHOU Song-ze, PENG Wen-fei, WANG Yong-gang. Effects of strain rate on mechanical properties, microstructure and texture of Al−Mg−Si−Cu alloy under tensile loading [J]. Transactions of Nonferrous Metals Society of China, 2020, 30: 27−40.

[10] DING Li-peng, JIA Zhi-hong, NIE Jian-feng, WENG Yao-yao, CAO Ling-fei, CHEN Hou-wen, WU Xiao-zhi, LIU Qing. The structural and compositional evolution of precipitates in Al−Mg−Si−Cu alloy [J]. Acta Materialia, 2018, 145: 437−450.

[11] LI Kai, BÉCHÉ A, SONG Ming, SHA Gang, LU Xing-xu, ZHANG Kai, DU Yong, RINGER S P, SCHRYVERS D. Atomistic structure of Cu-containing $\beta''$ precipitates in an Al−Mg−Si−Cu alloy [J]. Scripta Materialia, 2014, 75: 86−89.

[12] NINIVE P H, STRANDLIE A, GULBRANDSEN-DAHL S, LEFEBVRE W, MARIOARA C D, ANDERSEN S J, FRIIS J, HOLMESTAD R, LØVVIK O M. Detailed atomistic insight into the $\beta''$ phase in Al−Mg−Si alloys [J]. Acta Materials, 2014, 69: 126−134.

[13] WENG Yao-yao, JIA Zhi-hong, DING Li-peng, MURAISHI S, WU Xiao-zhi, LIU Qing. The multiple orientation relationships and morphology of $\beta'$ phase in Al−Mg−Si−Cu alloy [J]. Journal of Alloys and Compounds, 2018, 767: 81−89.

[14] FIAWOO M, GAO X, BOURGEOIS L, PARSON N, ZHANG X Q, COUPER M, NIE J F. Formation of multiple orientation relationships of $Q$ precipitates in Al−Mg−Si−Cu alloys [J]. Scripta Materialia, 2014, 88: 53−56.

[15] DING Li-peng, JIA Zhi-hong, WENG Yao-yao, LIU Ying-ying, WU Sai-nan, LIU Qing. The morphology and orientation relationship variations of $Q'$ phase in Al−Mg−Si−Cu alloy [J]. Materials Characterization, 2016, 118: 279−283.

[16] WENG Yao-yao, JIA Zhi-hong, DING Li-peng, DU Kui, DUAN Hui-chao, LIU Qing, WU Xiao-zhi. Special segregation of Cu on the habit plane of lath-like $\beta'$ and QP2 precipitates in Al−Mg−Si−Cu alloys [J]. Scripta Materialia, 2018, 151: 33−37.

[17] MARIOARA C D, ANDERSEN S J, STENE T N, HASTING H, WALMSLEY J, van HELVOORT A T J, HOLMESTAD R. The effect of Cu on precipitation in Al−Mg−Si alloys [J]. Philosophical Magazine, 2007, 87: 3385−3413.

[18] TORSÆTER M, LEFEBVRE W, MARIOARA C D,

ANDERSEN S J, WALMSLEY J C, HOLMESTAD R. Study of intergrown $L$ and $Q'$ precipitates in Al−Mg−Si−Cu alloys [J]. Scripta Materialia, 2011, 64(9): 817−820.

[19] KOLAR M, PEDERSEN K O, GULBRANDSEN-DAHL S, TEICHMANN K, MARTHINSEN K. Effect of pre-deformation on mechanical response of an artificially aged Al−Mg−Si alloy [J]. Materials Transactions, 2011, 52: 1356−1362.

[20] DING Li-peng, JIA Zhi-hong, LIU Ying-ying, WENG Yao-yao, LIU Qing. The influence of Cu addition and pre-straining on the natural aging and bake hardening response of Al−Mg−Si alloys [J]. Journal of Alloys and Compounds, 2016, 688: 362−367.

[21] ZHANG Yue, LING Juan, LI Hua-guan, LUO Xin-yi, BA Zhi-xin. Effect of pre-deformation and artificial aging on fatigue life of 2198 Al−Li alloy [J]. Materials Research Express, 2020, 7: 046509.

[22] SERIZAWA A, SATO T, MILLER M K. Effect of cold rolling on the formation and distribution of nanoclusters during pre-aging in an Al−Mg−Si alloy [J]. Materials Science and Engineering A, 2013, 561: 492−497.

[23] QUAINOO G K, YANNACOPOULOS S. The effect of prestrain on the natural aging and fracture behaviour of AA6111 aluminum [J]. Journal of Materials Science, 2004, 39: 4841−4847.

[24] BIROL Y, KARLIK M. The interaction of natural ageing with straining in a twin-roll cast AlMgSi automotive sheet [J]. Scripta Materialia, 2006, 55: 625−628.

[25] YASSAR R S, FIELD D P, WEILAND H. The effect of cold deformation on the kinetics of the $\beta''$ precipitates in an Al−Mg−Si alloy [J]. Metallurgical and Materials Transactions A, 2005, 36: 2059−2065.

[26] TEICHMANN K, MARIOARA C D, PEDERSEN K O, MARTHINSEN K. The effect of simultaneous deformation and annealing on the precipitation behaviour and mechanical properties of an Al−Mg−Si alloy [J]. Materials Science and Engineering A, 2013, 565: 228−235.

[27] TEICHMANN K, MARIOARA C D, ANDERSEN S J, MARTHINSEN K. The Effect of preaging deformation on the precipitation behavior of an Al−Mg−Si alloy [J]. Metallurgical and Materials Transactions A, 2012, 43: 4006−4014.

[28] SAITO T, MARIOARA C D, ANDERSEN S J, LEFEBVRE W, HOLMESTAD R. Aberration-corrected HAADF-STEM investigations of precipitate structures in Al−Mg−Si alloys with low Cu additions [J]. Philosophical Magazine, 2014, 94: 520−531.

[29] LAI Y X, FAN W, YIN M J, WU C L, CHEN J H. Structures and formation mechanisms of dislocation-induced precipitates in relation to the age-hardening responses of Al−Mg−Si alloys [J]. Journal of Materials Science & Technology, 2020, 41: 127−138.

[30] SAITO T, MARIOARA C D, RØYSET J, MARTHINSEN K, HOLMESTAD R. The effects of quench rate and pre-deformation on precipitation hardening in Al−Mg−Si alloys with different Cu amounts [J]. Materials Science and Engineering A, 2014, 609: 72−79.

[31] SAITO T, MURAISHI S, MARIOARA C D, ANDERSEN S J, RØYSET J, HOLMESTAD R. The effects of low cu additions and predeformation on the precipitation in a 6060 Al−Mg−Si alloy [J]. Metallurgical and Materials Transactions A, 2013, 44: 4124−4135.

[32] SUNDE J K, MARIOARA C D, HOLMESTAD R. The effect of low Cu additions on precipitate crystal structures in overaged Al−Mg−Si(−Cu) alloys [J]. Materials Characterization, 2020, 160: 110087.

# 预变形对 Al−Mg−Si−Cu 合金析出相结构和形成机制的影响

翁瑶瑶[1,2]，贾志宏[3,4]，丁立鹏[3]，廖 琎[1]，张萍萍[1]，徐亚琪[1]，刘 庆[3,4]

1. 南京工程学院 材料科学与工程学院，南京 211167；
2. 南京工程学院 江苏省先进结构材料与应用技术重点实验室，南京 211167；
3. 南京工业大学 先进轻质高性能材料研究中心，南京 211816；
4. 重庆大学 材料科学与工程学院 轻合金材料国际合作联合实验室(教育部)，重庆 400044

**摘 要：**基于原子分辨率的高角环形暗场扫描透射电子显微镜（HAADF-STEM）系统研究预变形对 Al−Mg−Si−Cu 合金中析出相结构和形成机制的影响。在预变形合金中，沿位错处形成拉长和线状的析出相。在位错处形成的析出相具有以下 3 个特征：析出相内部呈非周期性原子排列；Cu 原子偏聚发生在析出相/α(Al)的界面处；在一个析出相内部具有多种不同的取向。提出异质形核析出相的 4 种形成机制：被拉伸的析出相在位错上独立形成；线状析出相在位错上直接析出；不同的析出相相遇结合成线状析出相；析出相与其他相或溶质原子富集区相连接。这些不同的形成机制导致形成具有不同结构和形貌的析出相。

**关键词：**Al−Mg−Si−Cu 合金；预变形；Cu 偏聚；析出相；HAADF-STEM

**(Edited by Wei-ping CHEN)**